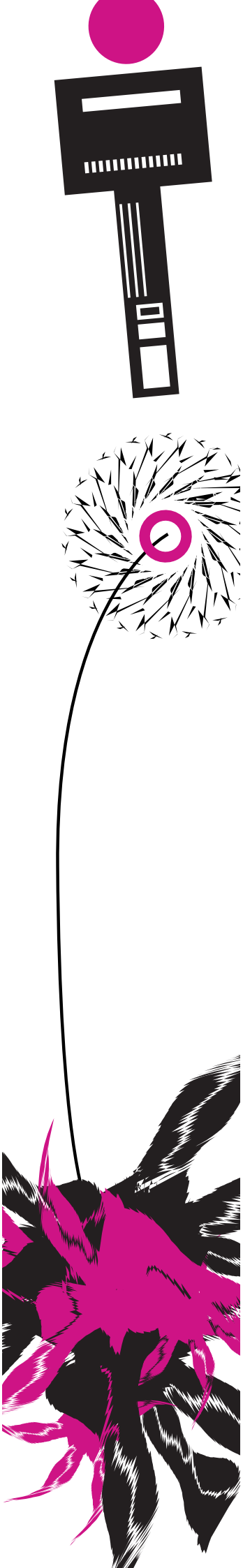

Bachelor's Thesis Biomedical Engineering

Design of a surgical manipulator using smart materials

Welmoed W. A. Tjepkema

Supervisor:	Prof. dr. S. Misra
Daily supervisor:	T.L. Thomas, PhD candidate

Report number: BE-807

June 28, 2021

Surgical Robotics Lab,
Engineering Technology - Biomechanical Engineering,
Faculty of Science and Technology

UNIVERSITY OF TWENTE.

Abstract

Objective. Minimally invasive surgery (MIS) is a method where surgery is performed through tiny incisions in the human body, rather than through large openings. This improves the recovery time of the patient and the risk of infection. A surgeon can perform MIS by bringing a surgical tool into to body of the patient to inspect the surrounding tissue or to deliver a drug or object to the target location. These surgical tools do not have an interface that allows for the steering of the tool once it has been introduced into the human body. Uncontrolled steering of a surgical tool can result in damage to the tissue of the patient and longer operation times. The steering of these tools is therefore highly reliant on a surgeon's skill. To improve the steering of these surgical tools, a new design for a so-called 'surgical manipulator' has been developed with the use of smart materials.

Methods. The use of shape memory alloys (SMAs) and shape memory polymers (SMPs) has been investigated for the development of a new surgical manipulator. Four concepts have been generalised with the use of SMAs which are actuated through the joule heating effect. The difference between the implementation of the one way shape memory effect (OWSME) and the two way shape memory effect (TWMSE) has been explored. Calculations on the shape memory effect, the critical shear stress, the achievable bending angle, the joule heating effect and the cooling down time have been made on the final design. Theoretically calculations are compared with the results from simulations of the final design, which are made in Comsol 5.5.

Results. The final design consists of three SMA springs which are programmed for the TWSME. Both the model of Liang and Rogers as well as the model of Lagoudas (the model which is used in Comsol) show the shape memory effect in SMAs. The maximum critical shear stress for a SMA spring of 10 mm long is 183 MPa, which results in a maximum displacement of 2.61 mm. A bending angle between 21.09° - 22.65° and 12.54° - 13.60° have been achieved for a surgical manipulator without and with a silicon rubber shell respectively. With a current of 0.55A, it takes about 1.7 seconds for the SMA springs to heat up through joule heating, and about 6 seconds to cool down again.

Conclusions. In this study a new design for a surgical manipulator has been proposed with the use of SMAs. The manipulator is able to bend in six different directions with a satisfactory heating and recovery time. With the use of this design more accurate steering of surgical tools is possible, which will result in faster operation times and less tissue damage to the patient.

Keywords: Shape memory alloys (SMA), surgical manipulator, smart materials, one way shape memory effect (OWSME), two way shape memory effect (TWSME), joule heating

Abstract (Nederlands)

Doelstelling. Minimaal invasieve chirugie vindt plaats door kleine sneetjes te maken in het menselijk lichaam, in tegenstelling tot de traditionele chirugie waarbij grote openingen in het lichaam worden gemaakt. Minimaal invasieve chirugie zorgt ervoor dat de hersteltijd van de patiënt korter wordt en de kans op infecties wordt verlaagd. Een chirurg brengt tijdens deze operatie een chirurgisch hulpmiddel in het lichaam om weefsel te kunnen inspecteren of om een object op een bepaalde plek in het lichaam te plaatsen. Het probleem met huidige chirurgische hulpmiddelen is dat ze niet door middel een interface worden aangestuurd, waardoor de besturing van deze hulpmiddelen afhankelijk is van de ervaring van de chirurg. Ongecontroleerde besturing van een hulpmiddel kan schade aan het weefsel van de patiënt aanbrengen en de operatieduur verlengen. Om de besturing van deze hulpmiddelen te verbeteren zal in dit verslag een nieuw ontwerp voor een zogenoemde 'chirugische manipulator' worden ontwikkelend met behulp van slimme materialen.

Methode. Het gebruik van geheugenlegeringen (in het engels ook wel shape memory alloys, of SMAs genoemd) of geheugenpolymeren (shape memory polymers, SMPs) is onderzocht voor de ontwikkeling van een nieuwe chirurgische manipulator. Vier concepten zijn gegeneraliseerd met het gebruik van SMAs die geactiveerd worden door het joule-effect. Het verschil tussen implementatie van het eenrichtingsgeheugeneffect en het tweeweg geheugeneffect is onderzocht. Op het gekozen ontwerp is het geheugeneffect, de kritische schuifspanning, de haalbare buigingshoek, het joule-effect en de afkoeltijd onderzocht. Theoretsiche berekeningen worden vergeleken met simulaties gemaakt in Comsol 5.5.

Resultaten. Het gekozen ontwerp bestaat uit drie SMA veren die geprogrammeerd zijn voor het tweeweg geheugeneffect. Zowel het model van Liang en Rogers als het model van Lagoudas (het model dat in Comsol wordt gebruikt) tonen het geheugeneffect in SMAs aan. De maximale kritische schuifspanning voor een SMA veer van 10 mm lang is 183 MPa, wat resulteert in een maximale verplaatsing van 2.61 mm. Voor een chirurgische manipulator met en zonder een siliconen bedekking is respectievelijk een buiging gehaald van tussen de 12.54° - 13.60° en 21.09° - 22.65°. Bij een stroomsterkte van 0.55A duurt het ongeveer 1.7 seconden voordat de SMA veren door het joule-effect zijn opgewarmd. Het duurt ongeveer 6 seconden voor de veren om weer af te koelen naar de omgevingstemperatuur.

Conclusies. In deze studie is een nieuw ontwerp voor een chirurgische manipulator voorgesteld met behulp van geheugenlegeringen. De manipulator kan in zes verschillende richtingen buigen met een gewenste reactiesnelheid. Met behulp van dit ontwerp kunnen chirugische instrumenten nauwkeuriger worden aangestuurd, wat resulteert in kortere operaties en minder weefselschade bij de patiënt.

Trefwoorden. geheugenlegeringen, chirurgische manipulator, slimme materialen, eenrichtingsgeheugeneffect, tweeweg geheugeneffect, joule effect

Preface

This thesis describes the findings of the research I carried out as part of my graduation study for the bachelor biomedical engineering, at the faculty of Science and Techology at the University of Twente. This research was part of the development of new macro designs in the Surgical Robotics Lab of the Biomechanical Engineering department. I thank my daily supervisor Theodosia L. Thomas (PhD candidate at the SRL) for giving me weekly feedback on my designs and introducing me to the topic of medical device design. I'm grateful for the opportunity I was given to learn to work with finite element software, which I had never worked with before. I also got the chance to improve my SolidWorks skills. I furthermore thank prof. dr. Sarthak Misra for his supervision and feedback, and ir. Edsko E. Hekman for his feedback on the designs.

Index

List of figures

List of Tables

1 Introduction

Minimally invasive surgery (MIS) has the benefits of performing surgery inside the body with fever and smaller incisions [3]. With MIS, both the risk of infection and the wound healing time are reduced. Furthermore, the diagnosis and patient treatment are improved [3]. Examples of minimally invasive procedures are endoscopy or microsurgery. A commonly used tool in MIS is a catheter, which is a long flexible tube which can be inserted into the vascular system, the gastrointensinal tract or the airway for diagnosis and treatment [3]. In figure 1 an example of a left heart catheterization is shown [4]. Surgical manipulators like a catheter are limited in their motion and are in continuous contact with the blood vessels, making it hard for the the distal end of the surgical manipulator to be controlled. This makes it more difficult to reach a target location inside the body. It can occur that the surgeon has to remove the surgical manipulator multiple times before the target location is reached, which results in small tissue traumas [5] [6] [7].

To reduce the risk of tissue trauma, research has been done on the fabrication of new steerable catheters, which allow for greater control of their movement in comparison to conventional catheters. Furthermore, the catheter stability in operation is improved and the total radiation exposure, where applicable, is reduced [3]. Examples of ways in which a surgical manipulator can be steered are with tendons, magnetic fields, soft materials and through hybrid actuation [3].

Smart materials like shape memory polymers (SMPs) or shape memory alloys (SMAs) are examples of materials which can contribute to the development of more accurate micro-actuators [8]. The benefits of using smart materials for the steering of a surgical manipulator are that they have super-plasticity, are biocompatible, have a high recoverable strain and a good steer-ability [3]. Acutation by SMAs are used more frequently as a replacement of actuation by electric motors, because motors still have the disadvantage of their weight and their bulkiness [9]. Other benefits of SMAs are their high force to weight ratio, their ability to be deformed by a simple current flow and that they don't make any noise [10]. They are currently already used in research for endoscopy applications [8] or in the actuation of a soft 3D printed robotic hand [9].

Because of the above benefits of smart materials, the focus of this study lies on the implementation of these materials in a new design for a surgical manipulator. In the next chapter, a brief summary on the working mechanisms of smart materials is given. In the chapters following up, a few concepts are shown, from which one concept is chosen as the final design for the surgical manipulator. This concept is simulated in a finite element software and conclusions on the implementation of the design are drawn at the end of this study.

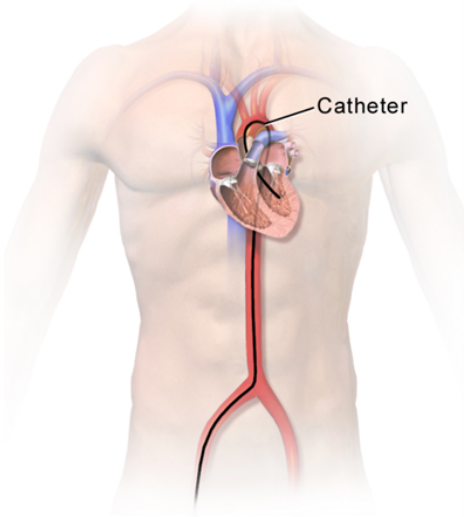

Figure 1: Schematic representation of the insertion of a catheter into the left atrium of the heart. The catheter has to be both flexible, to facilitate the following of the natural bends of the aorta, as well as limited in size, in order to fit into the vessels without causing trauma to the patient.

2 Theoretical background

A common form of smart materials are shape memory materials. These are materials which can change to a previous (memorized) form when an external stimulus is applied [11] [12]. This phenomenon is also called the shape memory effect (SME) [13]. Examples of external stimuli are heat, light or a magnetic field. There are many types of smart materials, shape-memory alloys (SMA) and shape memory polymers (SMP) are most commonly used.

2.1 Shape memory alloys

Shape-memory alloys are metallic alloys with the characteristics of a smart material. The alloys have two unique properties: pseudoelasticity and the shape memory effect (SME). Pseudoelasticity is the capability to exhibit a larger recoverable elongation upon mechanical loading, when compared to normal metals. Pseudoelasticity is the result of a stress-induced martensite transformation at constant temperature [2].

Metals are crystalline objects and their atoms are arranged in a regular space, which is also known as the crystal lattice. Normally when metals deform, the atoms trade places with each other in this crystal lattice. This movement is possible because electron bonds are broken, making the atoms free to move. This process is also called diffusion of the atoms. Another way by which a metal can deform is through slipping. This is also the primary mechanism behind plastic deformation. During slipping, bonds between large groups of atoms are broken, making it possible for the atom sheets to 'slip' over each other [14].

The shape memory effect is not caused by diffusion nor slipping of the atoms, but through an effect called martensitic transformation. The shape memory effect in SMA can occur in two different phases: the martensite and austenite phase. The chemical composition of the material will stay the same, the mechanical properties will however change during phase transition [2]. The martensite phase can be divided into two states: twinned martensite and detwinned martensite [11] [15].

At high temperatures the austenite structure is stable, whereas at low temperatures the martensite structure is stable [14]. Austenite has a very strong, cubic atomic structure, while martensite has more space between the atoms, and a structure which has a parallelogram shaped form. This difference in crystalline structure makes materials in their martensite phase more flexible and softer than materials in their austenite phase. When an external stimulus like heat is applied to a material in its martensite phase, the object will go back to its austenite phase (which is also called its programmed phase). Once the object has cooled down again it will go back to its twinned martensite phase. The material can then be brought into a new shape by applying a load or force on the object, which brings the object in a new deformed (or detwinned) martensite phase [11].

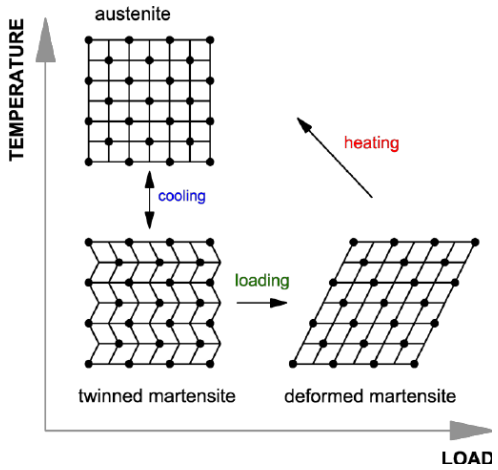

Figure 2: Schematic of the crystalline structures at twinned martensite, deformed martensite and austenite phase.

This process, which is also shown in figure 2 [16], can be repeated for a number of times. The process where the crystalline structure changes from a cubic structure to a parallelogram (twinned) structure, is called twinning. No atomic bonds are broken; the bonds can rotate and keep this shape after rotation. Because no bonds are broken, the material is capable of returning to its original shape.

The martensitic transformation can occur in two ways: thermally induced martensitic transformation and stress induced martensitic transformation. Stress induced martensitic transformation occurs when a certain amount of force or stress is exerted on the metal in its austenite phase. This stress will cause a transformation back to the martensitic phase. In this study, the focus lies on thermally induced martensitic transformation.

When heat is applied to a SMA object, the material will go from its martensite structure into an austenite structure. The temperature at which the material will enter the austenite phase is called the austenite-start-temperature (A_s) and the transition is finished at the austenite-finish temperature (A_f) [11] [17]. When the material is cooled down again, it will go back from its austenite state to its martensite phase. This process will start at the martensite-start-temperature (M_s) and will end at the martensite-finish-temperature (M_f). The difference between A_f and M_s is called hysteresis, which is caused by the need of a driving force to induce the transformation [2] [18]. For a surgical manipulator, a small hysteresis is preferred for fast actuation.

SMAs have great potential to replace actuators like electric motors and hydraulics [19]. A great choice for the alloy in a SMA is the nickel-titanium (NiTi) SMA, which can endure high stress and high external forces [7]. Besides NiTi, copper-zinc-aluminium (CuZnAl) and copper-aluminium-nickel (CuAlNi) are also frequently used. NiTi has a number of advantages over copper based alloys; NiTi has a large resistivity, a higher mechanical strength and a higher work density [17]. SMAs can be formed in multiple shapes, like thin plates or wires. They are able to execute a significant force [8]. The transformation temperatures depend on the composition of the alloy [11]. In general, NiTi exhibits the largest deformation recovery. Not only the transformation temperature depends on the composition of the alloy, other properties like fatigue life and flexibility are changed as well. The kelloggsresearchlabs made an overview of the impact of different additional elements to NiTi alloy, from which a summery is shown in in table 1 [14].

Table 1: Impact on the shape memory properties of the addition of different elements to the NiTi alloy

Additional element	Advantages	Disadvantages
Aluminium (Al)	Increases fatigue life and flexibility and reduces the weight.	
Cobalt (Co)	Recommended for applications which need a high stiffness	The shape memory effect is suppressed
Copper (Cu)	Decreases the thermal hysteresis (20% Cu results in a hysteresis of 2.5°C), allows a higher cylce rate and the TWSME is 5-7% enhanced.	Hard to produce, above 10% Cu SME starts to disappear, deformation should be limited to 3% for lower concentrations and the material gets a lower melting temperature
Hafnium (Hf)	Increases transition temperature	
Iron (Fe)	Stabilizes the transition temperature and increases the ultimate tensile strength to 4x of pure titanium	Decreases the transition temperature (around -40°C)
Magnesium (Mg)	Reduces the material stiffness and improves fatigue life	
Niobium (Nb)	Lightweight	Widens the thermal hysteresis
Palladium (Pd)	Increases the transition temperature	Expensive to produce
Platinum (Pt)	Increases the transition temperature	Expensive to produce

2.2 Shape memory polymers

Shape memory polymers are capable of fixing temporary shapes and recovering to the permanent shape upon activation by an external stimulus [1]. An example of commonly used SMP is polyurethane, which has a wide-ranging temperature for shape recovery and has a high recoverable strain (up to 400%) [20]. SMPs can be triggered by heat, light, magnetic field or a solution. SMPs consist of chain segments which are connected with physical or chemical netpoints. The netpoints provide stability and dictate the permanent shape of the material [12]. Chemical crosslinking occurs through covalent bonds, while physical crosslinking occurs thourgh intermolecular interactions.

The shape memory effect of SMPs is similar to that of SMAs. SMPs will go back to a programmed state after an external stimulus is applied. When the material is programmed, a temporary shape is made due to the incorporation of reversible netpoints. These netpoints prevent the chain segments from recoiling during deformation of the material. The programming of the material occurs under a high temperature. Under this high temperature, the material is deformed into a new shape. Next, the temperature is brought down. When the temperature is brought up again, the material will go back to its original shape. Depending on the material, a one-way shape-memory effect can occur or a reversible shape-memory effect. For the design of a SMP with a reversible shape memory effect, the design should incorporate two types of chain segments with distinctly different melt temperature ranges [12]. The mechanism of the shape memory effect of a SMP can be seen in figure 3, made by A. Lendlein and O. Gould [21].

There are two main types for printing a SMP into the desired shape; through polymemer jetting (by PolyJet) and through stereolithography. Other methods for printing the material are fused deposition modeling and hydrogel extrusion [12].

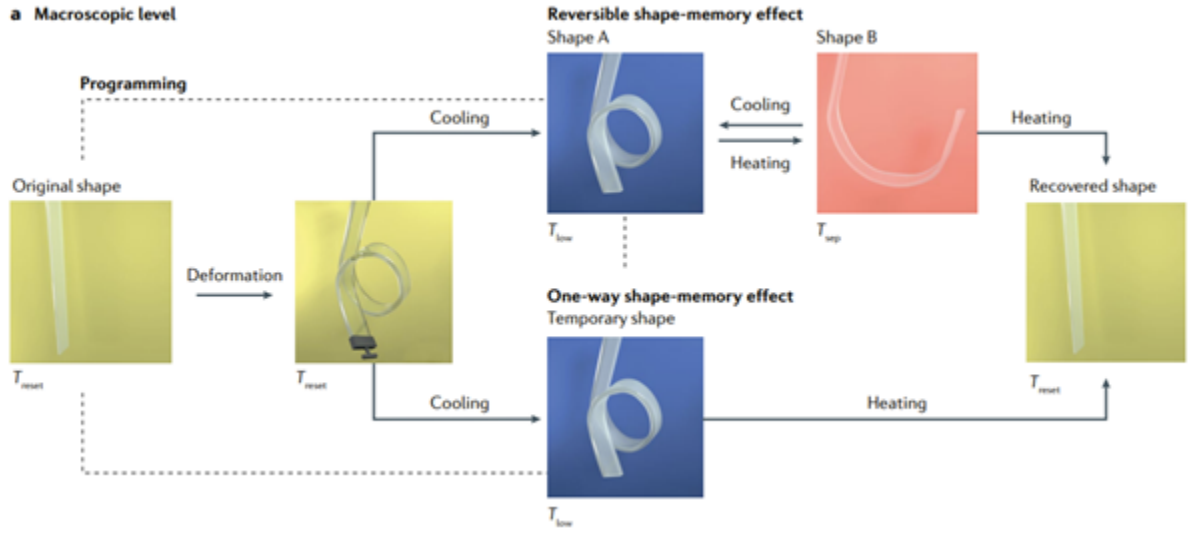

Figure 3: Programming of a coordinated physical response in polymeric systems, made by A. Lendlein and O.Gould. In the figure the reversible shape-memory effect and the one-way shape memory effect are shown.

3 Methods

3.1 Design requirements

The goal of this study is to make a new design for a surgical manipulator with the use of smart materials. In this study, only one segment of a surgical manipulator will be designed. This segment is the part of the surgical manipulator that when actuated will bend the manipulator to one direction. Multiple shapes of the surgical manipulator can be achieved when multiple bending segments are placed next to each other. One segment must meet the following requirements:

- *Bending angle.* The surgical manipulator has to be able to reach all the difficult anatomical destinations. In order to achieve this, the surgical manipulator should be able to bend in all directions. This requirement is also shown in figure 4.
- *Recovery.* The surgical manipulator should be able to be used multiple times. It is thus important that the segment is be able to recover back to its original form after it has been activated. Once the manipulator has reached its original position, it should be able to be actuated again to take on a new bending shape.
- *Size.* The diameter of the model should be as small as possible, preferably under 10 mm. A general diameter size for for example a catheter is between the 2.64 mm and 11.88 mm [22].
- *Reaction time.* The model should not react too quickly back to its original form, to avoid causing damage to the surrounding tissue. However, the model should also not react very slowly, because this increases the operation time, which is unfavourable for the surgeon and patient. For these reasons, a reaction time between 1 and 5 seconds is preferred.
- *Fabrication.* The model should be easy to fabricate with low assembly costs.

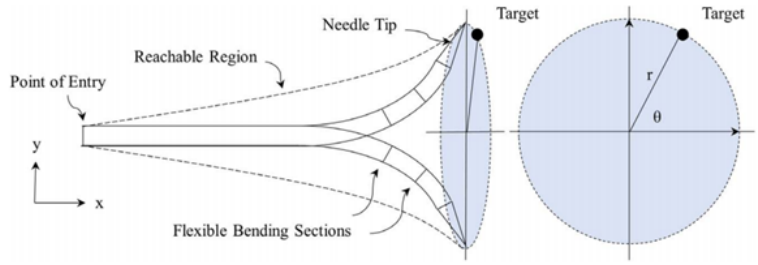

Figure 4: The manipulator should be able to bend in all directions [1]

3.2 Material selection

The bending angle of the manipulator depends on a few factors. A larger difference between the two temperatures of phases where SMA or SMP deform results in an increase of the resolution of the bending angle [23]. Shape memory polymers have the advantage of achieving a high stroke, are efficient, biodegradable and can sustain two or more shape changes [7] [21]. The biodegradable properties of SMP are interesting, and have been applied in research for implants and stents [12]. However, for the design of a new surgical manipulator, this property is not necessary. SMAs are preferred in applications which require higher actuation forces and a faster response time [23].

Another benefit of SMAs is that current can run through an SMA wire directly, thereby inducing the joule heating effect. This effect could be used to heat up the material. The joule heating effect can also be applied to SMPs which consist of conductive carbon nanofibers or carbon nanotubes. However, the fabrication method of these materials is difficult [24]. SMPs can also be heated by incorporation of a current carrying wire attached to the polymers, but this also complicates the design. The advantages and disadvantages of SMAs and SMPs are summarised in table 2. Due to the higher elastic modulus and quicker response time, shape memory alloys have been chosen to work with. A NiTi alloy will be implemented in the final design, since this alloy displays the largest deformation recovery rate in comparison to other alloys.

Table 2: Design benefits of SMAs compared to SMPs

Shape memory alloys			Shape memory polymers		
	Advantages	Disadvantages		Advantages	Disadvantages
+	High force to weight ratio	- Low strain (up to 10 % [2])	+	High strain (up to 700%)	- Low elastic modulus which results in a small recovery stress and force (4-10 MPa)
+	Can heat up directly through joule heating		+	Lower density	- Longer response time compared to SMAs
+	High elastic modulus (>400 MPa)		+	Lower processing costs	- Extra heating source has to be implemented in design
+	Quick response time		+	Easier fabrication than SMAs	

Multiple studies have investigated a new design for surgical manipulators with the use of SMAs. SMAs have been applied at new designs for an active catheter, for example in the research of Y. Haga [25], where they developed three kinds of active catheters with SMA coils. However, the recovery phase of the manipulator was not investigated. Coiled SMAs have also been used in the development of a soft 3D-printed robotic hand, where the fingers were controlled by a pair of coiled SMA muscles in a parallel antognistic setup. This concept can realize a 180 degree movement, but options for movements in 360 degrees still have to be explored. Another actuator was designed by Yeah-Hsun Lu et. al. [26], where only one SMA wire was wrapped around a needle. The fabrication of a design with only one SMA actuator is easier than a model with multiple SMA actuators, but it limits the surgical manipulator in the amount of bending directions [26]. In table 3 an overview of existing designs which incorporate SMA actuators is shown. Unfortunately, the two-way actuation (which includes the recovery phase after multiple working cycles) has been left out in most of these papers.

Table 3: Existing studies on steerable surgical manipulators with SMAs

Author (year)		number of SMA's	Bending angle	Outer diameter
G. Lim et al. (1995)	[27]	3 (small and coiled)	13°	2.8 mm
Y. Haga et al. (1998)	[25]	3 (small and coiled)	3 designs: 11° - 90°	2.0 mm
Y. Haga et al. (2000)	[28]	3	Torsional angle of 70°	1.4 mm
H. Takizawa et al. (1999)	[29]	3 (straight wires)	90°	1.5 mm
J. Szewczyk et al. (2011)	[30]	x (straight wires)	70°	1.2 mm

3.3 Shape of the shape memory alloys

The amount of force and displacement (or also referred to as the stroke) that a SMA actuator can exert depends on many factors, including the shape of the SMA. Straight wires as well as springs can be used as actuators. The main benefit of a straight wire is that it has a high material efficiency. Furthermore, due to the small total area, it doesn't weigh much and is also lower in costs. However, the biggest disadvantage is that a wire can't make large displacement. Depending on the amount of cycles used to program the material, the wire can only reach a displacement of 3-8% of it's original length.

Helical actuators on the other hand can achieve higher strokes [31] [9]. However, for these structures it is harder to calculate to displacement and other properties than for straight wires. Other properties which influence the force and displacement are for example the wire size, the pitch angle and the transition temperature. An increased wire size results in an increased force and decreased displacement of the actuator [31]. An increased pitch reduces the tensile motion and increases compressive motion. A higher transition temperature increases power consumption and heating time, but reduces the cooling time.

3.4 Actuation of shape memory alloys

The easiest way to actuate the SMAs is by applying heat to the material. This can be done by applying external heat to the surface of the material, or with the use of the joule heating effect or the Peltier effect. Since the surgical manipulator will be inside the body, the last two options are more preferable to avoid the heating of surrounding tissues.

Joule heating (which is named after its inventor James Prescott Joule) is the effect which occurs when a charge is passed through a electrical wire with a certain resistance. Due to the resistance of the wire, a certain amount of heat is released [32].

SMA materials can also be heated up by another thermoelectric effect, namely the Peltier effect [8]. This effect occurs when a current flows through the junction of two conductors (of different materials). The chemical difference between the two conductors causes the removal of heat at one junction, while at the other junction heat is deposited. This results in a temperature difference. This temperature difference can be used to heat up or cool down a material. The Peltier effect has the benefits that the air in nearby environment will not be heated up as much as with Joule heating, and that the electric consumption is lower. The Peltier effect has been applied in a research by J. Abadie, where they designed a new SMA micro-actuator for active endoscopy applications. However, in this research they managed to let the surgical manipulator only bend in one direction [8].

The Peltier effect would be able to reduce the cooling down time. However, this requires a more complicated design, which is not favourable for the fabrication method. For this study joule heating is chosen to actuate the SMA wires.

3.5 Programming SMAs

The production of a shape memory alloy is not easy. First of all, the composition of the alloy can change the transformation temperature. Secondly, a lot of equipment is needed to form the SMA in order to get the right properties. Lastly, the phase transformation behaviour is affected by shape-setting and heat treatments [12].
There are two kinds of shape memory effects: the one way shape memory effect (OWSME) and the two way shape memory effect (TWSME). Materials which exhibit the OWSME can recover to their programmed phase in austenite state. A material which is trained for the TSWME has two programmed states, it can remember its shape in austenite phase, but also in martensite phase [12]. In contrast to the OWSME, no external force is needed to retain a new shape in martensite phase. A schematic representation of the effects on microscopic (crystal structure) and macroscopic (the spring) scale can be seen in figure 5 and figure 6, made by A. Aalsma [2].

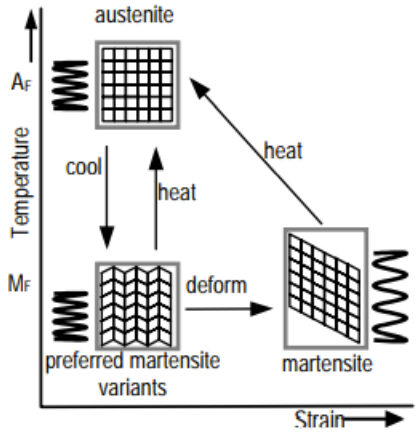

Figure 5: Schematic representation of the one way shape memory effect.

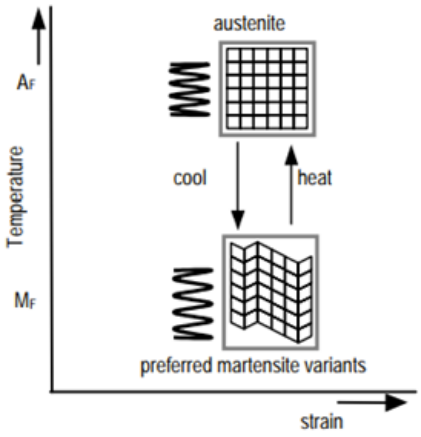

Figure 6: Schematic representation of the two way shape memory effect.

3.5.1 One way shape memory effect

The process of training a material for the OWSME is relatively simple in comparison to the TWSME effect. The training of a material for the shape memory effect often occurs with the use of a heat treatment. Since there are a lot of independent variables which influence the properties of NiTi, no mathematical model exists to predict the heat treatment of nitinol [14].

Two aspects should be considered when heat treatment of NiTi is applied: the right temperature and the right length of time. The thicker the diameter of a nitinol wire, the longer duration of heat treatment is required for rearranging the crystal structure. The longer the heat treatment, the stronger the shape memory effect will be. During heat treatment for the OWSME, the NiTi alloy will be held in a desired position for the austenite phase, while the temperature is raised to approximately 500-550°C for 30 minutes. The first heat treatment is called the initial heat treatment. During this phase, the material will be programmed into the desired shape. By applying a second heat treatment (called aging) the transition temperature can be risen. During the second heat treatment, the temperature will rise to 325-450 degrees. At these temperatures, the programmed shape is not re-set. The heat treatment can be performed by applying hot air, by heating in a controlled atmosphere, by induction and by heating in a vacuum [14].

3.5.2 Two way shape memory effect

The fabrication of the TWSME requires extra training steps. This can be done through mechanical and thermal treatment. There exist in general four methods for training the TWSME, which will be explained in this section. In all methods, all production cycles will be repeated multiple times [2]. A schematic overview of these four methods can be seen in figure 7 .

The first method to train the TWSME begins with deforming the material while keeping the temperature below M_f. As mentioned, M_f is the temperature where the martensite phase is finished. While the stress level is kept constant, the temperature is heated up above A_f (the temperature at which the austenite phase is finished) and then cooled down again to below M_f.
The second way to train a material for the TWSME is by heating the material up to above A_f and then deforming it until it reaches the end of its stress/strain plateau. While keeping the strain level constant, the temperature is switched from below M_f to above A_f.

The third method starts with deforming the material to its recoverable strain limit below the M_f temperature. When the applied stress is released, the temperature is heated up to above A_f and cooled down to below M_f.
In the fourth method the temperature is constant between A_f and Ms, and the material is deformed to its recoverable strain limit. In this way, the material will go into a stress-induced martensite phase. When the stress is released, the material returns to its austenite phase.

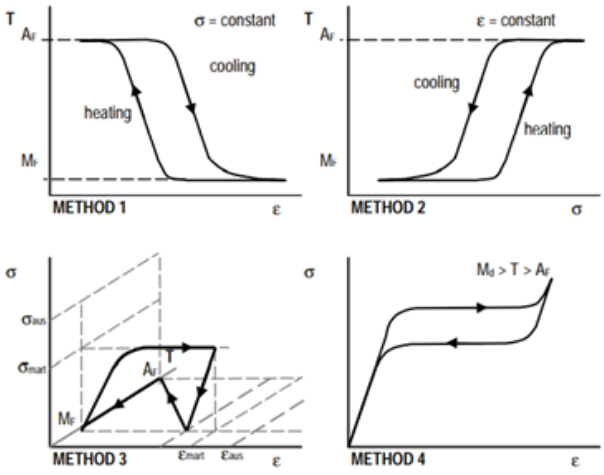

Figure 7: Schematic representation of the four methods which can be used to program a SMA for the TWSME [2].

3.6 Concepts

As stated in previous chapters, a shape memory alloy (NiTi) has been chosen to work with for in the final design. Four different concepts are made, with different shapes (straight wires and helical shaped wires) and different programming methods (OWSME and the TWSME). All SMAs will be actuated through joule heating.

In all concepts, 3 separated actuators (wires or springs) are placed. When one actuator is heated, it will contract until it reaches its programmed austenite state. When the actuator contracts, it will simultaneously bend the surgical manipulator to this direction. When two actuators are heated at the same time, the tube will bend in the direction of the midline between these two actuators. In this way, the surgical manipulator can bend in 6 different directions.

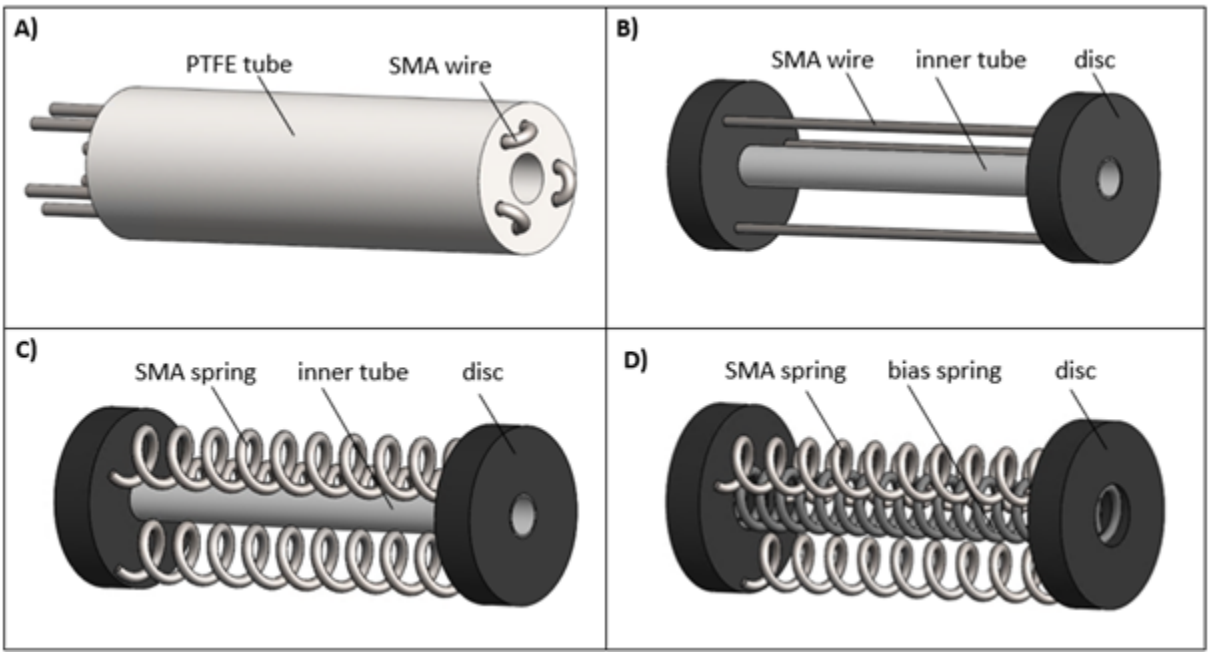

Figure 8: Different concepts for the surgical manipulator made in SolidWorks. **A** concept 1: three SMA wires, programmed for the TWSME, are enclosed in a PTFE tube. **B** Concept 2: three straight SMA wires, programmed for the TWSME, are attached with their ends to two discs. **C** Concept 3: three SMA springs, programmed for the TWSME, are attached with their ends to two discs. **D** Concept 4: three SMA springs, programmed for the OWSME, are attached with their ends to two discs. A central bias spring is implemented for recovery of the original position.

3.6.1 Concept 1: TWSME SMA wires enclosed in a PTFE tube

The first concept can be seen in figure 4A. In this concept, three SMA wires are enclosed inside a tube. A similar design has been made by Padasdao et al [1]. In this design, the wires don't make direct contact with the tissue, thereby preventing thermal tissue damage. Furthermore, the wires are looped back at the tip of the manipulator. This causes the bending forces of the manipulator to be doubled, and ensures that the wires can easily be connected to a positive and negative current at the bottom end of the manipulator. The inner radius of the shell is 1 mm, the outer radius of the shell is 2 mm. The diameter of a SMA wire is 0.25 mm. The soft material can be made of Nylon or PTFE (Teflon). The wires will be programmed for the TWSME.

3.6.2 Concept 2: TWSME SMA wires attached to discs

The second concept can be seen in figure 4B. One segment of the surgical manipulator consists of two discs of 1 mm thick. The diameter of a disc is 2 mm, with a central hole of 1.2 mm. Through this hole, a camera or a small tube can be inserted. The actuators are 3 straight SMA wires, which can achieve a strain up to 8% [33]. The springs will be programmed for the TWSME.

3.6.3 Concept 3: TWSME SMA springs attached to discs

The third concept can be seen in figure 4C. This concept is very similar to concept 2, however, the three straight wires are replaced by three SMA springs. The diameter of the discs is enlarged up to 4.4 mm, with a central hole of 1.2 mm. Due to the spring shaped form, a larger stroke can be achieved than with straight wires. The springs will be programmed for the TWSME.

3.6.4 Concept 4: OWSME SMA springs with a bias spring attached to discs

The last concept can be seen in figure 4D. This design consists of three OWSME SMA springs and one central bias spring made of stainless steel. When one SMA spring is heated it will contract, pulling the surgical manipulator to that direction. The spring will stop contracting when it has reached its austenite phase. When no current is supplied anymore, the spring will cool down again. The spring will be pulled back to its previous (stretched out) form, due its own elastic recovery and to the recovering force of the central bias spring.

In order to investigate if the bias spring in this concept is able to recover the position of the OWSME SMA springs, the following calculations are made. Yili Fu et al. designed a model for calculating the bending angle when a central bias spring is implemented (see figure 9) [34]. This mechanical model is expressed with the use of the model of H. Liu [35]. The output force of the SMA coil spring is equal to:

$$F = \frac{EI\theta}{eL} \tag{1}$$

where EI is the bending stiffness of the bias spring, θ is the bending angle, e is the offset of the SMA spring from the centre of the bias spring and L is the length of one bending unit.

The critical shear stress for a SMA coil spring actuator is equal to 183 MPa [31]. Knowing the critical shear stress value, the maximum force exerted on the SMA spring can be calculated using the following formula [36]:

$$\tau = \frac{8FD}{\pi d^3} + \frac{4F}{\pi d^2} \tag{2}$$

where τ is equal to the critical shear stress, F is equal to the force exerted on the spring, D is the diameter of the spring (1.5 mm) and d is the diameter of the spring wire (0.25 mm). From equation 2, a maximum force of 0.69 N is calculated.
The length on one bending segment is equal to 10 mm, and the offset of the SMA spring from the centre of the bias spring is 1.5 mm. From equation 1 it follows that the bending stiffness of the bias spring should be equal to 0.69 Nmm^2 to achieve a bending angle of 15°.

In order to calculate the bending stiffness of the bias spring, it is assumed that the bias spring is equivalent to a slender bar of the same length when bending laterally. Using this assumption, the equivalent bending rigidity of spring is given by:

$$EI = \frac{Ed^4L}{32(2+\mu)DN} \tag{3}$$

where E is the material's elastic modulus, and μ is the materials poisson ratio. For the material of the bias spring, stainless steel has been chosen. The elastic modulus of stainless steel is equal to 190 GPa and the poisson ratio is equal to 0,265 [37].

The diameter of the wire, diameter of the spring and the number of coils can be changed to achieve an bending stiffness of 0.69 Nmm^2. Following this formula, the bias spring should be designed with a large amount of coils, a large spring diameter or a small wire diameter. Since such a spring is difficult to design, this two-way actuation method is not preferred.

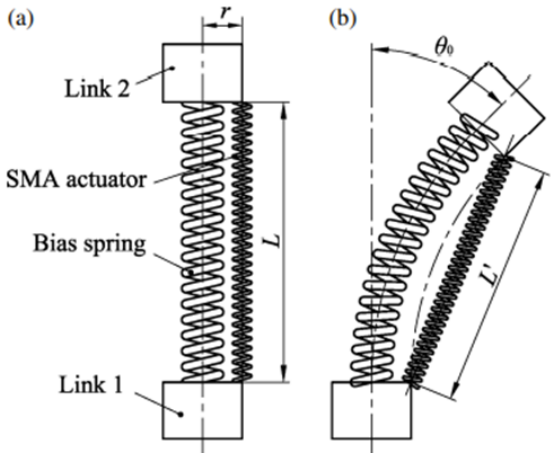

Figure 9: Schematic of a model with a central bias spring and a SMA spring. L is the original length a single SMA actuator, L' is the length when the SMA actuator is contracted, θ is the bending angle and r is the distance of the axis of the bias spring from the axis of the SMA actuator.

3.6.5 Concept selection

A final design is chosen from the previously described concepts. This is done by assigning weight factors to the required functions of the design, with numbers between 1 and 5. Here, the number 1 stands for a lesser important criteria and 5 stands for a very important criteria.
The concepts will be rated with grades between 0 and 5, where 0 means that the design does not complete the requirement and 5 means that the design completely fulfills the requirement. The concept grading can be seen in table 4. The total points for an concept can be calculated be multiplying each grade with the weight factor for that criteria, and adding all these points for the total result. An calculation example: concept 1 scores 3 points on the criteria 'achievable bending angle'. This criteria has a weight factor of 5 points, so concept 1 scores in total 15 points for this criteria.

Table 4: Concept grading

Criteria	Weight factor	Concept 1	Concept 2	Concept 3	Concept 4
Achievable bending angle	5	3	3	4	4
Achievable recovery	5	4	4	4	1
Recovery time	4	4	5	5	5
Easy fabrication method	2	2	2	2	3
Low cost assembly	1	2	3	3	4
Easy actuation	3	5	4	4	4
Multiple shapes possible	2	2	5	5	5
Size	2	5	5	4	4
Total	x	86	94	97	85

4 Results

Based on the weight grading from table 4, the final design for the surgical manipulator is based on concept 3. A SolidWorks model of how multiple segments can be inserted next to each other to form a whole surgical manipulator can be seen in figure 10. A sheet of silicon rubber (with a thickness of 0.1 mm) has been wrapped around the segments to prevent the hot SMA springs from touching the surrounding tissues. The inner tube is made of silicon rubber and has a thickness of 0.1 mm and an outer diameter of 1.2 mm. In this design, the electrical wiring has been left out. One segment of the surgical manipulator consists of two discs of 1 mm thick (which can be printed with a stereolithography printer from the University of Twente, using resin). The springs can be attached to the discs with adhesive or by automated crimping (in pocket-, concentric-, bended- and pressed on-form) [38]. The best way to sterilize the silicon rubber tube after usage is by ethylene oxide sterilization (EtO) treatments, which in comparison to Gamma Ray sterilization and steam autoclave has the least effect on the properties of the surgical manipulator [39].

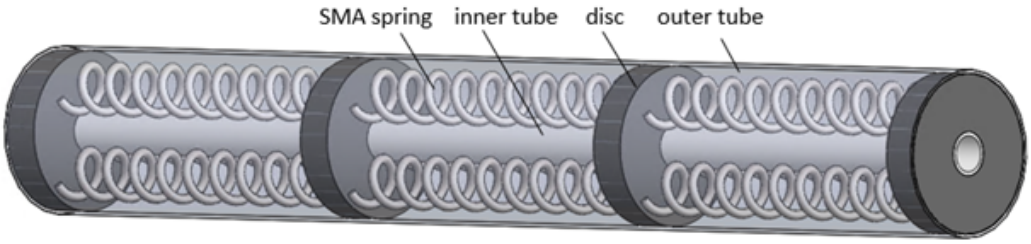

Figure 10: Final design of the surgical manipulator, based on concept 3. Three segments are placed next to each other, the whole surgical manipulator is covered with a silicone rubber shell to prevent the hot SMA springs from getting in contact with the surrounding tissue.

4.1 Comsol simulations of the shape memory effect

Simulations of the final model have been made in a finite element software. Comsol and Abaqus were compared during this study, eventually Comsol was chosen because this software is used more in the Surgical Robotics Lab. In Comsol the module 'Shape memory alloys' has been used to model the pseudoelasticity and the shape memory effect of Nitinol. The material properties of Nitinol (in its austenite and martensite phase), silicone rubber and resin can be found in table 7, 8 and 9 respectively in Appendix B.

The properties of Nitinol are dependent on the alloy composition and the fabrication method. In literature there exist many different values for the Young's modulus and the thermal conductivity for Nitinol. The values from table 7 are primarily based on the study of Veláquez and Pissaloux [40] and Sung-Min An et al [31]. Here, the Martensite phase finishes at 315K [42°C], starts at 325K [52°C] and the austenite phase starts at 341K [68°C] and ends at 351K [78°C].

To investigate the transition from martensite to austenite phase in the shape memory effect, the austenite volume fraction is plotted in Comsol (which uses the model of Lagoudas [11]) and is theoretically calculated using the model of Liang and Rogers, which is described in equation 4 [40]:

$$\xi = \begin{cases} 0, & T > A_f \\ \frac{1}{2}[\cos(\pi \frac{T-A_s}{A_f-A_s}) + 1] & A_s < T < A_f \\ 1, & T < A_s \end{cases} \tag{4}$$

In figure 11 these two models are compared. The model of Lagoudas (in Comsol) has a more linear relation than the model of Liang and Rogers. The input conditions for this Comsol simulation can be found in table 10 in Appendix B. As can be seen in the figure, the percentage of the austenite volume fraction is dependent on the temperature. In between the martensite starting temperature and the Austenite starting temperature is a state where both phases can coexist. In this figure, the hysteresis between cooling and heating can also be seen [2].

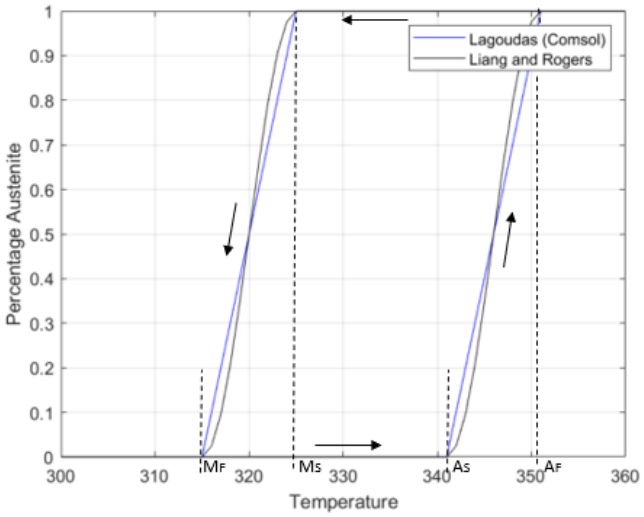

Figure 11: Comparison between the calculated percentage austenite volume with the Lagoudas (Comsol) model and with the model of Liang and Rogers. M_s, M_f, A_s and A_f stand for the martensite and austenite start and finish temperatures respectively.

4.2 Shear stress and maximum displacement

The critical shear stress for a SMA coil spring actuator is equal to 183 MPa [31]. Using equation 2, a maximum force of 0.69 N is calculated. With the force, the possible displacement can be calculated [36]:

$$y = \frac{F}{k} \tag{5}$$

where k is the spring coefficient. K can be calculated using the following formula [36]:

$$k = \frac{d^4 G}{8 D^3 N} \tag{6}$$

where G is equal to the the shear modulus (18.26 GPa in austenite phase [31]), and N is the number of coils of the spring (in this model N = 10).
As can be seen from formula 5 and 6, the displacement of the spring is dependent on the diameter of the spring and wire, and the number of coils. As can be seen in figure 12, a spring diameter of 3 mm can even result in a stroke over 100%. For the wire of this model a diameter of 0.25 mm and a spring diameter of 1.5 mm has been chosen. This results in a maximum displacement of 2.61 mm.

When one spring contracts, the springs on the opposite side will be stretched out a little. To prevent the spring from stretching out too much and thereby crossing the critical stress limit, the maximum contraction of a spring is limited to 2.20 mm.

With the maximum displacement decreased and the springs implemented in the model, the maximum shear stress in Comsol can be calculated. The input for this Comsol simulation can be found in table 11 in Appendix B. The calculated shear stress of the model is dependent on the mesh in Comsol. The finest mesh the computer could calculate was extra fine, which gave a maximum shear stress of 134 MPa, as can be seen in figure 13.

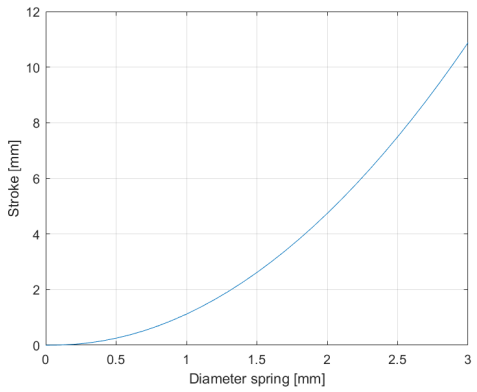

Figure 12: Influence of the diameter of the spring on the stroke.

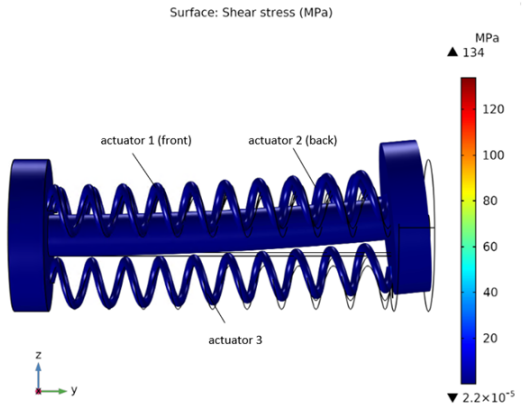

Figure 13: Comsol model of the total shear stress, when spring 1 and 2 are actuated.

4.3 Achievable bending angle

Bending angles could be calculated in Comsol by applying applying a displacement of the calculated 2.20 mm on each of the actuators. The spring is stretched out in the martensite phase, and compressed (from a total length of 10 mm to 7.80 mm) in the austenite phase. The input for this Comsol simulation can be found in table 11 in Appendix B. The achievable bending angles with and without silicon rubber tube after one working cycle are shown in table 5. The average bending angle of the surgical manipulator without a silicon rubber tube is between 21.09° and 22.65°. The bending angles for a surgical manipulator which is covered with a silicon rubber tube is between the 12.54° and 13.60°. In figure 14 and figure 15 the simulations of the possible displacement of the surgical manipulator in Comsol are shown.
In this design, the SMA springs are programmed for the TWSME. Literature showed that for a SMA spring, the recovery rate after 200 working cycles is decreased to 60%. After 1000 working cycles, the TWSME reaches a stable recovery rate of 45% [41].

Table 5: Achievable bending angels with and without silicon rubber tube after 1 working cycle.

Actuator	Without tube	With tube
1	21.09°	12.75°
1 and 2	22.47°	13.60°
2	21.33°	12.87°
2 and 3	21.33°	13.09°
3	21.14°	12.54°
3 and 1	22.65°	13.16°

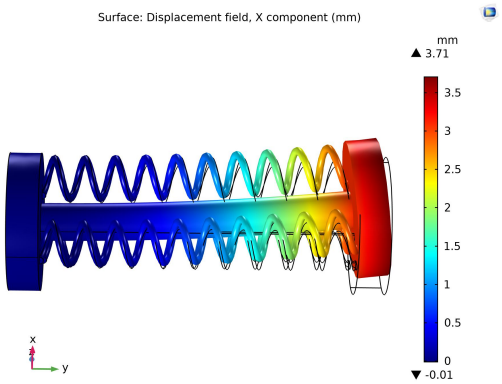

Figure 14: Comsol simulation of displacement of the surgical manipulator without silicon rubber tube.

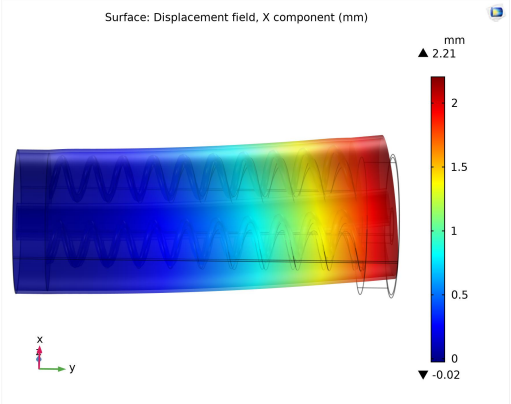

Figure 15: Comsol simulation of displacement of the surgical manipulator with silicon rubber tube.

4.4 Joule heating effect

The SMA springs are actuated through the joule heating effect. The resistance of a wire is dependent on the kind of material and the diameter of the wire. When Joule heating is applied, the power of heating generated is equal to the product of the square of the current and the resistance [40] [42]:

$$P = I^2 R \tag{7}$$

The resistance can be calculated as follows [42]:

$$R = \rho L / A \tag{8}$$

where ρ is the resistivity of the material, L is the length of the wire and A is the area of the wire. The area of the wire can be calculated as follows:

$$A = \pi d^2 \tag{9}$$

Here d is the diameter of the wire [42]. Following this formula, the cross-sectional area of the wire is equal to 0.05 mm^2. The length of the wire can be calculated using the following formula:

$$L = n\sqrt{C^2 + p^2} \tag{10}$$

where C is equal to $D\pi$ and p (the pitch) is equal to height of one segment divided by the number of coils, which is equal to 1 mm. Using this formula, the length of a SMA spring is equal to 48.17 mm.

The electrical resistivity is equal to the inverse of the electrical conductivity, which is equal to 8e-4 Ωmm for the martensite phase and 1e-3 Ωmm for the austenite phase. The resistance of the SMA spring in martensite and austenite phase can be calculated using equation 8, which results in 0.77Ω and 0.96Ω respectively. Using equation 7, the power of heating for the martensite phase is equal to 0.069 J/s and for the austenite phase 0.086 J/s.
The difference in temperature in the SMA spring can be calculated with the power of heating as follows:

$$dT = \frac{Q}{mC_p} \tag{11}$$

where m is the mass of the spring (=1.24e-5 kg) and C_p is the heat capacity of Nitinol, which is 320 $J/(kgK)$.

The temperature after a certain amount of time is equal to the original temperature (298 K) plus the temperature difference. The effect of joule heating on the temperature of the SMA spring over time can be seen in figure 16. For these calculations, a current of 0.30A has been chosen. An increase in current results in a faster heating time. During the process of joule heating, the wires cool down simultaneously by convection. A more accurate simulation of the joule heating effect in Comsol can thus be seen in figure 17. For these simulations, a current of 0.55A has been applied through the spring. The SMA reaches its austenite finish temperature (of 351K) within 1.7 seconds. The input conditions for Comsol for these simulations can be found in table 12 in Appendix B.

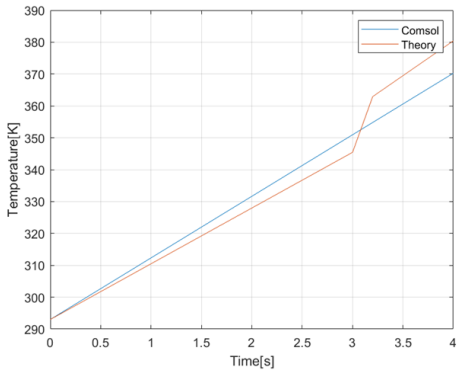

Figure 16: Theoretically calculated temperature versus the calculated temperature by Comsol, I = 0.30A.

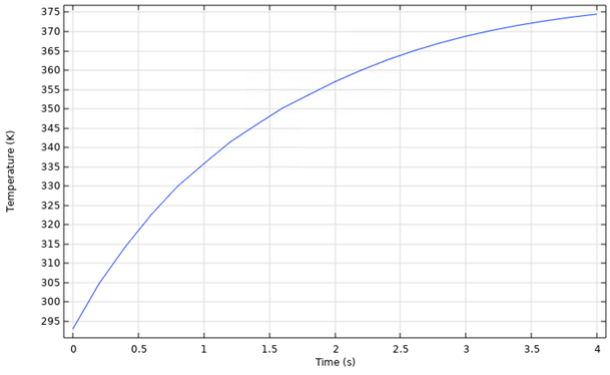

Figure 17: Comsol simulation of the joule heating effect and the impact of heat convection, I = 0.55A.

4.5 Cooling phase of SMA

In surgery, a long operating time is undesirable. Therefore, in the design of an actuator composed of shape memory materials, it is important to consider the recovery time. Normally, cooling of the material takes places by natural convection or conduction. To speed up the recovery time, a cooling system can be added in the design. The time it takes for the material to cool down and go back to its deformed state is dependent on multiple parameters, like the size and the shape of the actuator. The diameter of the wire is also important, as actuators with a small diameter heat up faster due to a higher resistivity and cool down faster because they have a higher surface-to-volume ratio [7]. The effect of the diameter of the wire can also be seen in table 6 in appendix A of this paper, based on the NiTi from Dynalloy [19]. Besides shape and size of the actuator, the response time is also dependent on the stress applied on the material and the loading conditions [10]. Suitable methods to cool a SMA material are fluid flow and heat sinking [10]. Fluid flow has for example been applied in the design of a novel artificial muscle, where the SMA spring bundle was heated and cooled with hot and cold water [43].

To investigate if a extra cooling system is necessary to design in the surgical manipulator, some thermodynamic calculations are made for a simplified model of the manipulator. A shape memory alloy can lose heat by radiation, conduction or convection. Under the temperature of 100 °C, radiation can be ignored [17].
The heat transfer through the surgical manipulator can be modeled by a series of resistors, as can be seen in figure 18. For simplification, the design has been modeled as a straight wire in a cylinder of air, which is surrounded by a layer of silicon rubber.

The resistance of the air can be modeled as [44]:

$$R_{air} = \frac{\ln \frac{r_2}{r_1}}{2\pi K_a L} \tag{12}$$

where r_2 is the inner radius of the silicone rubber shell (=2.2 mm), r_1 is the radius of the SMA wire (=0.125 mm) and K_a is the thermal conductivity of air (=2.4e-4 W/mmK). Using this formula, it follows that the heat resistance of air is equal to 1901.83 K/W.
The heat resistance of the silicon rubber can be modeled in a same way:

$$R_{rubber} = \frac{\ln \frac{r_3}{r_2}}{2\pi K_s L} \tag{13}$$

where r_3 is the outer radius of the silicon tube (=2.3 mm), and K_s is the thermal conductivity of silicon rubber (=2.2e-4 W/mmK). It follows that the heat resistance of rubber is equal to 3.22 K/W.
The resistance as a consequence of convection between the silicon rubber and blood (which for now will be modeled as water) can be calculated using the following formula [44]:

$$R_{conv} = \frac{1}{hA} \tag{14}$$

where h is the heat transfer coefficient of water (=1e-3 W/mm^2K) and A is the surface area of the silicon tube (=144.51 mm^2). It follows that the heat resistance by convection is equal to 6.92 K/W.

The total heat resistance is equal to the sum of the resistance of air, rubber and convection, which is 1911.97 K/W in total. Given that the mean temperature is of blood is 310 K, the steady rate of heat loss can be calculated by dividing the temperature difference between the austenite finish (=351 K) temperature and the temperature of blood by the total resistance, which gives a heat loss of 0.021 W.

The temperature difference due to the presence of air is equal to the product of the heat loss times the resistance of air, which is 40.8 K. Due to the joule heating effect, the temperature of the air will thus become 351-40.8 = 310.2K. The martensite phase will start not start till 341 K, so an additional cooling system does not have to be implemented.

Without a silicon tube, the total heat resistance will be equal to the heat resistance which occurs due to convection between the SMA wire and blood. Following from equation 14 and implementing the heat coefficient of NiTi (= 94.96 *10^-6 W/mm^2) and surface area of the wire (=7.85 mm^2), gives a resistance of 1341.50 K/W. The steady heat loss than becomes 0.031 W.

The cooling down time of a SMA spring can be calculated using the following formula:

$$T = T_0 + (T - T_0)\exp(-\lambda t) \tag{15}$$

where T_0 is the environment temperature (=298K), λ is equal to:

$$\lambda = \frac{Ah}{pVC} \tag{16}$$

In this equation, h is the heat transfer coefficient for NiTi, p is the density of NiTi (=6450kg/m^3) and C is the heat capacity of NiTi (=320J/(kgK). The surface area (A) is read from the SolidWorks model, which is equal to 31.32 mm^2. The comparison between the cooling down time of the spring in Comsol and the cooling down time calculated with equations 15 and 16 can be seen in figure 19. The input conditions for the Comsol simulations of the cooling down time can be found in table 13 in Appendix B. As can be seen in figure 19, it takes about 6 seconds for the SMA spring to cool down from its austenite finish temperature (of 351K) to the environmental temperature (which in this case is equal to the temperature of blood, which is on average 310K).

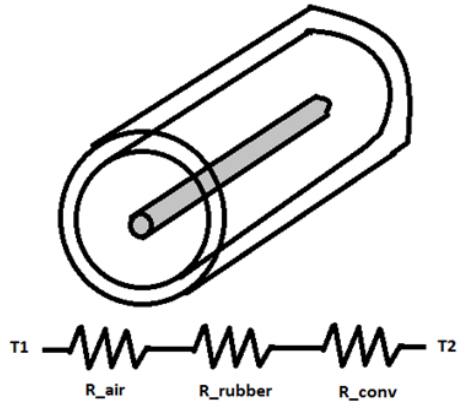

Figure 18: Schematic of simplified model for thermodynamic calculations.

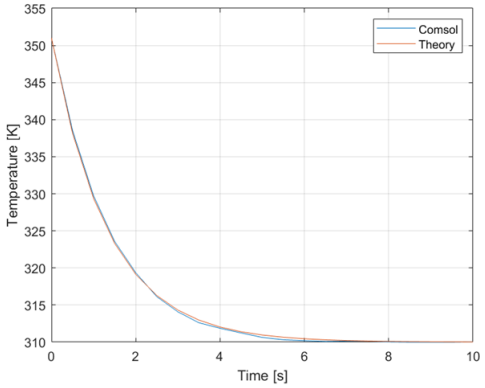

Figure 19: Comparison between theoretical calculations and Comsol simulations of the cooling down time of a SMA spring in air.

5 Discussion

In this study a new design for a surgical manipulator has been proposed with the use of smart materials. The requirements for the design have been met as closely as possible. In this section, the requirements and achieved results will be discussed, as well as some applications for this design will be given.

5.1 Achieved bending angle

The first requirement was that the surgical manipulator should be able to bend in all directions. The final design of this study is not able to bend in all directions, it can however bend in 6 different directions from the original position by activating one or two SMA springs through joule heating. Changing the amount of current which runs through the wire would only affect the reaction time. Bending angles between 21.09° - 22.65° and 12.54° - 13.60° for a 10 mm long segment of surgical manipulator without and with a silicon rubber tube wrapped respectively around could be achieved. The addition of a silicon rubber tube decreases the achievable bending angle significantly (by almost 10°). It also contributes to an increase in the stress of the surgical manipulator. The thickness of the silicone tube could be further decreased from 0.1 mm to 7.5 µm [45].

5.2 Position recovery after bending of the surgical manipulator

The second requirement for the surgical manipulator was that it should be able to be used for multiple times. It is thus important that the segment is be able to recover back to its original form after it has been activated. The final design is able to recover back to its original position, when the SMA springs are programmed for the TWSME. The recovery rate of the TWSME decreases with the number of working cycles. After 200 working cycles a recovery rate can be achieved up to 60% and the recovery rate reaches a stabilization of 45% after more than 1000 working cycles. This will cause the bending angle of one segment of the surgical manipulator without a silicone rubber cover to decrease to an average of 13.12° and 9.84° after more than 200 and 1000 working cycles respectively. For a surgical manipulator with a silicone rubber cover, the average bending angle decreases to 7.84° and 5.88° after more than 200 and 1000 working cycles.

5.3 Size

The third requirement for the surgical manipulator is that its diameter should be as small as possible, preferably under the 10 mm. The diameter of the surgical manipulator with silicone rubber cover is equal to 4.6 mm. It is furthermore possible to reduce the diameter of the surgical manipulator even further, by leaving out the links of the design, and attaching the components directly to the inner tube with adhesive [25].

5.4 Reaction time

The fourth requirement for the design was a not too slow, but also a not too fast reaction time of the manipulator. When a current of 0.55A is run through the SMA springs, a spring can achieve the austenite finish temperature of 351K within 1.7 seconds. By changing the amount of current running through the SMAs, the actuation time of the springs can be speeded up or slowed down.

In section 4.5 of this thesis, the impact of an silicone rubber cover on the heat distribution of the surgical manipulator has been investigated. The addition of a silicone rubber cover to the surgical manipulator decreases the heat loss from 0.031 W to 0.021 W. The temperature of the air surrounding the SMA wire will heat up to 310.2K. This is however not enough to heat up the other SMA wires to their austenite starting temperature (which is equal to 341K). An additional cooling system does not have to be implemented in the design. The cooling down time of a single SMA spring was modeled in Comsol. It takes about 6 seconds for a SMA spring to cool down from its austenite finish temperature to the temperature of the environment (which is 310K in the simulations, the temperature of blood).

The calculations were based on a model with a straight SMA wire in an empty segment surrounded by a silicon rubber tube. This is however not completely aligned with the final design model. Furthermore, heat transfer through conduction through the link has not been investigated. The design of a more accurate thermodynamical model was outside the scope of this study, if however it turned out the that an

additional cooling system is necessary, the design should be slightly adjusted. The heating of the wires through joule heating could be exchanged for heating the wires through the Peltier effect. Furthermore, the thickness and shape of the silicon tube could be adjusted or fins could be added. Other ways to increase the cooling rate could be by forced-air convection, oil cooling or water cooling [40] [19].

5.5 Fabrication

The last requirement for the design was that the model should be easy to fabricate with low assembly costs. The design uses SMA springs which are programmed for the TWSME. The TWSME is in general more difficult to produce and more expansive than SMA springs programmed for the OWSME. The TWSME requires a lot of training and equipment, it is therefore recommended to contact companies which custom produce SMAs in spring form with the TWSME. Examples of these companies are Dynalloy, Kelloggsresearchlabs and Biometal fiber. In general is a biometal fiber more flexible than flexinol (from the company Dynalloy) [10]. Each company has its own way of programming the material for the OWSME and the TWSME. Producing the TWSME is the hardest and most expensive part of producing this design of the surgical manipulator. It has however still the preference over the OWSME, because better recovery of the original position of the surgical manipulator can be achieved.

To cover the surgical manipulator with the silicone tube, the tube first has to be swelled in liquid n-hexane. Once the tube is swelled, the surgical manipulator is inserted into the tube. After this, the silicone tube is dried at room temperature rapidly, causing the tube to shrink. This will cause the tube to be strangled to the discs of the surgical manipulator [45].

As mentioned in section 4 'Results', the SMA springs can be attached to the discs with adhesive or by automated crimping (in pocket-, concentric-, bended- and pressed on-form) [38]. The discs can be attached to the inner tube by using non-conductive epoxy (for example from Torr Seal, Varian Vacuum Products) [45]. The discs can be printed with a stereolithography printer from the University of Twente, using resin.

The wires will be heated up through joule heating. In the current design, electrical wiring has been left out. To implement electrical wiring for all segments of the surgical manipulator, holes in the disks should be designed where the wires can run through.

5.6 Application

This design can be used for multiple usages in surgery. One example is for micro-endoscopy, by adding a small camera which runs through the inner tube. An example of such a camera can be the Misumi color CMOS camera B1000 [46]. The diameter of this camera is 0.91mm, the camera length itself is 1.168 mm and the diameter of the tube is 0.65mm. The addition of a camera to this surgical manipulator will however contribute to the overall stiffness of the tube, which can result in an decrease in the achievable bending angle.

Another application of this surgical manipulator can be to serve as a catheter. By adding multiple bending segments next to each other, different shapes of the manipulator can be achieved. This design for a new surgical manipulator enables easier steering of the catheter in comparison to traditional catheters. Difficult located anatomical structures are therefore easier to reach than with traditional catheters.

6 Conclusion

In this study a new design for a surgical manipulator has been proposed with the use of smart material. A new design is needed to better facilitate the in-use bending of surgical manipulators. To achieve this, the working mechanisms for both shape memory alloys and shape memory polymers have been investigated. Due to its material properties, SMAs have been chosen as actuators for the final design. The wires are heated up through joule heating and trained to exhibit the two way shape memory effect. Four concepts were designed in this study, from which one design consisting of two discs and three SMA springs has been chosen as the final design.

With a critical shear stress of 183 MPa, a maximum displacement of 2.61mm for a 10 mm long spring could be achieved. This resulted in bending angels between 21.09° - 22.65° and 12.54° - 13.60° for the surgical manipulator without and with a silicon rubber tube wrapped around respectively. These bending angels account for a 10 mm long segment, when multiple segments are placed next to each other greater bending angles will be possible. The wires are trained for the two way shape memory effect, so that a recovery rate after 200 working cycles can be achieved up to 60% and the recovery rate reaches a stabilization of 45% after more than 1000 working cycles.

The total diameter (with silicon rubber tube) is 4.6 mm, which is below the requirement of 10 mm. The SMA springs can be heated up to the austenite finish temperature within 1.7 seconds at a current of 0.55A, and cool down in 6 seconds to the environmental temperature. The proposed design meets most of the set requirements. Where requirements weren't met, alternatives have been proposed as future work.

This design can be used for multiple applications in surgery. One example is for micro-endoscopy, by adding a small camera which runs through the inner tube. Another application of this surgical manipulator can be to serve as a catheter. This design for a new surgical manipulator enables easier steering of the catheter in comparison to traditional catheters. Difficult located anatomical structures are therefore easier to reach than with traditional catheters. With this design, tissue traumas due to inaccurate steering of traditional surgical tools will be decreased and the total operation time will be shorted.

References

[1] Padasdao B, Konh B. Shape Memory Alloy Actuators in an Active Needle - Modeling, Precise Assembly, and Performance Evaluation. Journal of Manufacturing Science and Engineering, Transactions of the ASME. 2021;143(2). doi:10.1115/1.4047737.

[2] Aalsma A. Design of a linear shape memory alloy actuator. In: The iLLeD. Design of an intramedullary Leg Lengthening Device; 2000. .

[3] Hu X, Chen A, Luo Y, Zhang C, Zhang E. Steerable catheters for minimally invasive surgery: a review and future directions. Computer Assisted Surgery. 2018;23(1):21–41. doi:10.1080/24699322.2018.1526972.

[4] Blaus B. Medical gallery of Blausen Medical 2014. WikiJournal of Medicine. 2014;1(2). doi:10.15347/wjm/2014.010.

[5] Reisner LA, King BW, Klein MD, Auner GW, Pandya AK. A prototype biosensor-integrated image-guided surgery system Raman spectroscopy. The International Journal of Medical Robotics and Computer Assisted Surgery. 2007;3(1):82–88. doi:10.1002/rcs.

[6] Marchandise E, Flaud P, Royon L, Blanc R, Szewczyk J. Thermal and hydrodynamic modelling of active catheters for interventional radiology. Computer Methods in Biomechanics and Biomedical Engineering. 2011;14(7):595–602. doi:10.1080/10255842.2010.489044.

[7] Mohd Jani J, Leary M, Subic A, Gibson MA. A review of shape memory alloy research, applications and opportunities. Materials and Design. 2014;56:1078–1113. doi:10.1016/j.matdes.2013.11.084.

[8] Abadie J, Chaillet N, Lexcellent C. Modeling of a new SMA micro-actuator for active endoscopy applications. Mechatronics. 2009;19(4):437–442. doi:10.1016/j.mechatronics.2008.11.010.

[9] Deng E, Tadesse Y. A soft 3d-printed robotic hand actuated by coiled sma. Actuators. 2021;10(1):1–24. doi:10.3390/act10010006.

[10] Tadesse Y, Thayer N, Priya S. Tailoring the response time of shape memory alloy wires through active cooling and pre-stress. Journal of Intelligent Material Systems and Structures. 2010;21(1):19–40. doi:10.1177/1045389X09352814.

[11] Lagoudas DC. Alloys, Shape Memory. Texas A&M University; 2006. doi:10.1007/978-0-387-47685-8.

[12] Lee AY, An J, Chua CK. Two-Way 4D Printing: A Review on the Reversibility of 3D-Printed Shape Memory Materials. Engineering. 2017;3(5):663–674. doi:10.1016/J.ENG.2017.05.014.

[13] Petrini L, Migliavacca F. Biomedical Applications of Shape Memory Alloys. Journal of Metallurgy. 2011;2011(Figure 1):1–15. doi:10.1155/2011/501483.

[14] Kellog J. Nitinol in plain language;. Available from: `https://www.kelloggsresearchlabs.com/`.

[15] Rastogi R, Pawar SJ. A computational study of shape memory effect and pseudoelasticity of NiTi alloy under uniaxial tension during complete and partial phase transformation. Materials Research Express. 2019;6(5). doi:10.1088/2053-1591/ab06e1.

[16] Górski M. Active monitoring with use of smart structures based on high-strength fibre composites as a method of structural elements optimisation. 2013.

[17] Reynaerts D, Van Brussel H. Design aspects of shape memory actuators. Mechatronics. 1998;8(6):635–656. doi:10.1016/S0957-4158(98)00023-3.

[18] Mihálcz I. Fundamental characteristics and design method for nickel-titanium shape memory alloy. Periodica Polytechnica Mechanical Engineering. 2001;45(1):75–86.

[19] Arias Guadalupe J, Copaci D, Serrano del Cerro D, Moreno L, Blanco D. Efficiency Analysis of SMA-Based Actuators: Possibilities of Configuration According to the Application. Actuators. 2021;10(3):63. doi:10.3390/act10030063.

[20] Canyon Hydro, Summary E, Of F, Potential THE, Ferreres XR, Font AR, et al. We are IntechOpen , the world ' s leading publisher of Open Access books Built by scientists , for scientists TOP 1 %. Intech. 2013;32(July):137–144.

[21] Lendlein A, Gould OEC. Reprogrammable recovery and actuation behaviour of shape-memory polymers. Nature Reviews Materials. 2019;4(2):116–133. doi:10.1038/s41578-018-0078-8.

[22] Newman DK. Indwelling Urinary Catheters: Types; 2013. Available from: `https://www.urotoday.com/urinary-catheters-home/indwelling-catheters/description/types.html`.

[23] Ayvali E, Liang CP, Ho M, Chen Y, Desai JP. Towards a discretely actuated steerable cannula for diagnostic and therapeutic procedures. International Journal of Robotics Research. 2012;31(5):588–603. doi:10.1177/0278364912442429.

[24] Lu H, Liu Y, Gou J, Leng J, Du S. Electroactive shape-memory polymer nanocomposites incorporating carbon nanofiber paper. International Journal of Smart and Nano Materials. 2010;1(1):2–12. doi:10.1080/19475411003612749.

[25] Haga Y, Tanahashi Y, Esashi M. Small diameter active catheter using shape memory alloy. Proceedings of the IEEE Micro Electro Mechanical Systems (MEMS). 1998:419–424.

[26] Lu YH, Mani K, Panigrahi B, Hajari S, Chen CY. A Shape Memory Alloy-Based Miniaturized Actuator for Catheter Interventions. Cardiovascular Engineering and Technology. 2018;9(3):405–413. doi:10.1007/s13239-018-0369-7.

[27] Lim G, Minami K, Sugihara M, Uchiyama M, Esashi M. Active catheter with multi-link structure based on silicon micromachining. Proceedings of the IEEE Micro Electro Mechanical Systems. 1995:116–121. doi:10.1109/memsys.1995.472543.

[28] Haga Y, Esashi M, Maeda S. Bending, torsional and extending active catheter assembled using electroplating. Proceedings of the IEEE Micro Electro Mechanical Systems (MEMS). 2000:181–186. doi:10.1109/memsys.2000.838513.

[29] Takizawa H, Tosaka H, Ohta R, Kaneko S, Ueda Y. Act ˆ Bending Equipped With Mi % Tactile. Time:412–417.

[30] Szewczyk J, Marchandise E, Flaud P, Royon L, Blanc R. Active catheters for neuroradiology. Journal of Robotics and Mechatronics. 2011;23(1):105–115. doi:10.20965/jrm.2011.p0105.

[31] An SM, Ryu J, Cho M, Cho KJ. Engineering design framework for a shape memory alloy coil spring actuator using a static two-state model. Smart Materials and Structures. 2012;21(5). doi:10.1088/0964-1726/21/5/055009.

[32] Yan H, Wu H. Joule Heating and Chip Materials. Encyclopedia of Microfluidics and Nanofluidics. 2015. doi:10.1007/978-1-4614-5491-5.

[33] Koh JS. Design of shape memory alloy coil spring actuator for improving performance in cyclic actuation. Materials. 2018;11(11). doi:10.3390/ma11112324.

[34] Fu Y. Research on the axis shape of an active catheter. The International Journal of Medical Robotics and Computer Assisted Surgery. 2008;4:69–76. doi:10.1002/rcs.172.

[35] Liu H, Fu Y, Yan Z, Wang P, Wang S. A dynamic model for the active catheter actuated by the shape memory alloy coil spring. 2009 IEEE International Conference on Mechatronics and Automation, ICMA 2009. 2009;(August):1968–1973. doi:10.1109/ICMA.2009.5244978.

[36] Jenkins H. Extension & Torsion Springs. Mercer University;. Available from: `http://faculty.mercer.edu/jenkins_he/documents/SpringsCh10ExtensionTorsionsprings.pdf`.

[37] Materials A. Stainless steel - Grade 304 (UNS S30400);. Available from: `https://www.azom.com/properties.aspx?ArticleID=965`.

[38] Dynalloy. Automated crimping - Improve qualtity and streamline your production line;. Available from: `https://www.dynalloy.com/crimps.php`.

[39] Zhou H, Moua Y, Sayadeth I, Reski T. Sterilization Effects on Rubber Materials. Journal of Medical Devices. 2021;6(1). doi:10.1115/1.4026688.

[40] Velázquez R, Pissaloux EE. Modelling and temperature control of shape memory alloys with fast electrical heating. International Journal of Mechanics and Control. 2012;13(2):3–10.

[41] Zu X, Wang Z, Yu H. Two-way shape memory coil springs: design, actuation, and stability. International Conference on Smart Materials and Nanotechnology in Engineering. 2007;6423(May):64232H. doi:10.1117/12.779876.

[42] Olafsen LJ, Jones B, Sparks L, Nguyen HH, Tanner A, Schubert KE, et al. Current-controlled Nitinol wire for improved arterial navigation. 2019;(February 2019):40. doi:10.1117/12.2511670.

[43] Park CH, Choi KJ, Son YS. Shape memory alloy-based spring bundle actuator controlled by water temperature. IEEE/ASME Transactions on Mechatronics. 2020;24(4):1798–1807. doi:10.1109/TMECH.2019.2928881.

[44] Cengel Y, Ghajar A. Heat and Mass transfer: Fundamentals and Applications; 2014.

[45] Mineta T, Mitsui T, Watanabe Y, Kobayashi S, Haga Y, Esashi M. Batch fabricated flat meandering shape memory alloy actuator for active catheter. Sensors and Actuators, A: Physical. 2001;88(2):112–120. doi:10.1016/S0924-4247(00)00510-0.

[46] Misumi. Ultra mini CCQ II color camera manual;.

[47] Castelo Ferreira P, Pascoal-Faria P, Carreira P, Alves N. A Computer Simulation of the Nitinol Thermal Expansion under Fast Varying Working Conditions. Applied Mechanics and Materials. 2019;890(May):162–173. doi:10.4028/www.scientific.net/amm.890.162.

[48] DYNALLOY inc . Technical Characteristics of FLEXINOL ® Actuator Wires Table of Contents Makers of Dynamic Alloys NICKEL - TITANIUM ALLOY PHYSICAL PROPERTIES. 2013:1–12.

[49] Designerdata D. Silicone rubber data;. Available from: `https://designerdata.nl/materials/plastics/rubbers/silicone-ubber`.

[50] Wolf A, Descamps P. Determination of Poisson's ratio of silicone sealants from ultrasonic and tensile measurements. ASTM special technical publication. 2002:132–142.

[51] Formlabs Inc . Material Data Sheet Clear. WwwFormlabsCom. 2016:3–5. Available from: `https://formlabs.com/media/upload/Clear-DataSheet.pdf`.

[52] Saseendran S, Wysocki M, Varna J. Cure-state dependent viscoelastic Poisson's ratio of LY5052 epoxy resin. Advanced Manufacturing: Polymer and Composites Science. 2017;3(3):92–100. doi:10.1080/20550340.2017.1348002.

[53] Vuki. Impregnants resins Vupos.

Appendix

A. Influence of diameter size of a SMA wire

Table 6: Properties of the SMA wires (Dynalloy)

Diameter Size (mm)	Force (N)	Cooling Time 70 °C (s)	Cooling Time 90 °C (s)
0.025	0.0089	0.18	0.15
0.038	0.02	0.24	0.2
0.050	0.36	0.4	0.3
0.076	0.80	0.8	0.7
0.100	1.43	1.1	0.9
0.130	2.23	1.6	1.4
0.150	3.21	2.0	1.7
0.200	5.70	3.2	2.7
0.250	8.91	5.4	4.5
0.310	12.80	8.1	6.8
0.380	22.50	10.5	8.8
0.510	35.60	16.8	14.0

B. Input conditions for the Comsol simulations

Table 7: Comsol material properties of NiTi

Property		Martensite value	Austenite value
Thermal conductivity	[47]	8.6 W/(m K)	18 W/(m K)
Heat capacity at constant pressure	[40]	320 J/(kg K)	320 J(kg K)
Young's modulus	[31]	16.26 GPa	42.55 GPa
Electrical conductivity	[48]	1.25e6 S/m	1.00e6 S/m
Relative permittivity		1	1
Density	[48]	6450 kg/m^3	6450 kg/m^3
Poisson ratio	[48]	0.33	0.33

Table 8: Comsol material properties of silicone rubber

Property		Value
Young's modulus	[49]	3 MPa
Poisson's ration	[50]	0.49
Density	[49]	1250 kg/m^3

Table 9: Comsol material properties of resin

Property		Value
Young's modulus	[51]	1.6 GPa
Poisson's ration	[52]	0.35
Density	[53]	1050 kg/m^3

Table 10: Comsol simulation input for the austenite volume fraction plot on a SMA spring (results shown in figure 11)

Condition	Value
Initial strain	-0.22
Shape memory alloy Temperature	parametric sweep (300:1:360)
Shape memory alloy reference temperature	298 K
Shape memory alloy transformation temperatures	Ms=325 K; M_f = 315 K; A_s= 341 K; A_f = 351 K
Shape memory alloy slope of martensite and austenite curve [15]	7.4 MPa/K
Mesh	Fine

Table 11: Comsol simulation input for shear stress (shown in figure 13) and displacement (shown in figure 14 and figure 15) calculations on final design

Condition	Selected component	Value
Initial strain	selected actuator	-0.22
Fixed contraint	bottom of the lower segment and inner tube	
Mesh for displacement	-	Fine
Mesh for shear stress	-	Extra fine

Table 12: Comsol simulation input for plotting of the joule heating effect (shown in figure 16 and figure 17 on a SMA spring)

Condition	Value
Initial strain	-0.22
Shape memory alloy Temperature	Temperature (ehm 1)
Parameter T_{amb}	298 K
Shape memory alloy reference temperature	T_{amb}
Shape memory alloy transformation temperatures	Ms=325 K; M_f = 315 K; A_s= 341 K; A_f = 351 K
Shape memory alloy slope of martensite and austenite curve [15]	7.4 MPa/K
Parameter Iin	0.3 A (figure 16) or 0.55 A (figure 17)
Electric current Terminal	Iin
Convective heat flux coefficient (for figure 17)	94.96 W/(m^2K)
Convective heat flux external temperature (for figure 17)	T_{amb}
Mesh	Fine

Table 13: Comsol simulation input for plotting of the cooling down time (shown in figure 19 on a SMA spring)

Condition	Value
Initial strain	-0.22
Shape memory alloy Temperature	351 K
Parameter T_{amb}	310 K
Shape memory alloy reference temperature	T_{amb}
Shape memory alloy transformation temperatures	Ms=325 K; M_f = 315 K; A_s= 341 K; A_f = 351 K
Shape memory alloy slope of martensite and austenite curve [15]	7.4 MPa/K
Convective heat flux coefficient (for figure 17)	94.96 W/(m^2K)
Convective heat flux external temperature (for figure 17)	T_{amb}
Mesh	Fine